Lab on a Chip

RSC Publishing

PAPER

View Article Online
View Journal | View Issue

Cite this: *Lab Chip*, 2013, **13**, 1790

Integrated acoustic immunoaffinity-capture (IAI) platform for detection of PSA from whole blood samples†

A. Ahmad Tajudin,[ah] K. Petersson,[a] A. Lenshof,[a] A.-M. Swärd-Nilsson,[c] L. Åberg,[c] G. Marko-Varga,[a] J. Malm,[b] H. Lilja[bdei] and T. Laurell*[afg]

Received 17th November 2012,
Accepted 27th February 2013

DOI: 10.1039/c3lc41269e

www.rsc.org/loc

On-chip detection of low abundant protein biomarkers is of interest to enable point-of-care diagnostics. Using a simple form of integration, we have realized an integrated microfluidic platform for the detection of prostate specific antigen (PSA), directly in anti-coagulated whole blood. We combine acoustophoresis-based separation of plasma from undiluted whole blood with a miniaturized immunoassay system in a polymer manifold, demonstrating improved assay speed on our Integrated Acoustic Immunoaffinity-capture (IAI) platform. The IAI platform separates plasma from undiluted whole blood by means of acoustophoresis and provides cell free plasma of clinical quality at a rate of 10 uL/min for an online immunoaffinity-capture of PSA on a porous silicon antibody microarray. The whole blood input (hematocrit 38–40%) rate was 50 μl min^{-1} giving a plasma volume fraction yield of ≈33%. PSA was immunoaffinity-captured directly from spiked female whole blood samples at clinically significant levels of 1.7–100 ng ml^{-1} within 15 min and was subsequently detected *via* fluorescence readout, showing a linear response over the entire range with a coefficient of variation of 13%.

Introduction

On-chip detection of low abundant protein biomarkers is of interest to enable point-of-care (POC) diagnostics. However, detecting the biomarkers of interest directly from whole blood samples presents a high degree of complexity[1] such as interference or non-specific binding from the cellular elements in blood.[2] In addition, biomarker targets may only be present at low abundance, are rapidly degraded or eliminated by other mechanisms *in vitro*. Still, blood serum and plasma remain the most widely used biofluids in clinical diagnostics due to the fact that the blood/plasma biomarker profile reflects physiological and pathological changes relating to disease.[3,4] Although conventional immunoassays/antibody-validation assays, such as ELISA, have been the golden standard in clinical diagnostics, improvements with regards to time, sample/reagent consumption, portability and throughput are imperative. To implement a total LOC platform, the challenge lies not only in dealing with the sample complexity but also the sensitivity and specificity of the subsequent diagnostic assay, which needs to be simultaneously tackled. With regards to the needs of realizing a total LOC platform, developments using microfluidic technology have opened new possibilities for the detection of disease-correlated biomarkers from complex biological samples such as blood/plasma[5–8] and urine.[9,10] Many of the recent advancements in microfluidic-based lab on a chip approaches that target POC settings[11,12] involve efforts towards full system integration, increased throughput, multiplexing, cost-efficiency, rapid 'sample to answer', miniaturized immunoassay systems. Reports on microfluidic immunoassay platforms using diffusion,[13,14] surface/beads-immobilized,[15,16] centrifugal[17,18] and other separation-based approaches,[19,20] demonstrate rapid progress in miniaturizing conventional immunoassays, taking into account the complexity of the unprocessed, whole blood samples.

Reduction of the sample complexity due to interference from blood cells in whole blood samples is crucial to ensure a low limit of detection for the biomarkers of interest. In this

[a]*Department of Measurement Technology and Industrial Electrical Engineering, Lund University, Box 118, 22100, Lund, Sweden*
[b]*Department of Laboratory Medicine, Division of Clinical Chemistry, Skåne University Hospital (SUS), 20502, Malmö, Sweden*
[c]*Clinical Immunology and Transfusion Medicine, University and Regional Laboratories, Region Skåne, Lund, Sweden*
[d]*Department of Laboratory Medicine, Surgery (Urology), and Medicine (GU-Oncology), Memorial Sloan-Kettering Cancer Center, New York, NY10065, USA*
[e]*Institute of Biomedical Technology, University of Tampere, Finland*
[f]*Department of Biomedical Engineering, Dongguk University, Seoul, Korea*
[g]*CREATE Health, BMC D13, Lund University, Lund, Sweden*
[h]*Faculty of Biotechnology and Biomolecular Sciences, Universiti Putra Malaysia, 43400 UPM Serdang, Selangor, Malaysia*
[i]*Nuffield Department of Surgical Sciences, University of Oxford, Oxford, United Kingdom*

† Conflict of interest: Dr Hans Lilja holds patents for free PSA, hK2 and intact PSA assays.

case, separation-based microfluidics relies on the capability of the system to perform efficient on-chip separation of plasma by removing the blood cells prior to immunoaffinity-capturing of the targeted biomarkers. For example, several studies specifically utilizing membrane filters,[21,22] the Zweifach-Fung effect[19,23] (bifurcation law) and acoustophoresis-based separations[24] have shown successful combinations of on-chip separations and immunoassays. Being able to handle high cellular content *e.g.* undiluted blood, these approaches offer a potential for the development of fully-integrated microfluidic whole-blood immunoassay platforms.

We herein present an integrated microfluidic platform that uses acoustophoresis to extract plasma from whole blood and performs simultaneous immunoaffinity-capturing of a prostate cancer biomarker within 15 min. We have previously reported on an acoustophoresis-based microchip, which was capable of generating diagnostic quality anti-coagulated plasma from undiluted whole blood samples.[24] It was further linked to a potential clinical application by measuring prostate-specific antigen (PSA) off-line on a porous silicon sandwich antibody microarray chip. In this work, we have proceeded to develop an integrated device where the porous silicon microarray chip was connected directly to the outlet of the plasmapheresis chip, namely, the Integrated Acoustic Immunoaffinity-capture (IAI) platform.

Materials and methods

Proteins and reagents

Prostate Specific Antigen (PSA) was obtained from Sigma. Anti-PSA monoclonal mouse antibodies 2E9 and H117 were produced and characterized as previously described.[25,26] 2E9 monoclonal antibody was labelled with fluorescein isothiocyanate (FITC) isomer I-Celite (Sigma, St. Louis, MO, USA) and separated on a PD10 column (Amersham, Uppsala, Sweden).

Blood samples

Citrated blood samples from healthy female blood donors were obtained from Blood Center Skåne (Lund University Hospital, Sweden). The hematocrit level of the whole blood samples were measured by a hematocrit centrifuge (Hematocrit 210, Hettich, Tuttlingen, Germany). To determine the red blood cell content of the plasma samples after acoustic separation, a Coulter counter (Multisizer 3, Beckman Coulter Inc., Fullerton, CA) was used to count cells in the range of 4-8 μm.

For analysis, a titration series of PSA-spiked female whole-blood samples was made in the range of 1–100 ng ml^{-1}. As a reference, fractions of the spiked whole blood samples were centrifuged for plasma separation prior to determination of total PSA concentration, using DELFIA Prostatus PSA free/total assay, a commercially available quantitative time-resolved fluoroimmunoassay targeting both free and total PSA (Perkin-Elmer, Turku, Finland).[27]

IAI platform

The IAI platform has two major components:

1) the acoustic plasmapheresis microchip

2) the porous silicon microarray for on-chip immunoaffinity-capturing of PSA.

Both components were integrated in a polymer manifold encompassing both the plasmapheresis microchip and a flow cell holding the porous silicon PSA microarray.

Acoustic plasmapheresis microchip fabrication. Briefly, the acoustic plasmapheresis microchip consists of a meander microchannel with a whole blood inlet, four blood cell waste outlets (outlets A–D, Fig. 1) and one plasma outlet (outlet E, Fig. 1). The four waste outlets were centred at the bottom along the microchannel. A more detailed description of the acoustic plasmapheresis chip has been reported by Lenshof *et al.*[24]

The immunoaffinity-capture region: porous silicon microarray fabrication. Porous silicon chips were obtained by anodic dissolution of a p-type monocrystalline silicon wafer. A detailed description of the fabrication process has been reported by Järås *et al.*[28]

Monoclonal mouse anti-PSA capture antibody H117 (0.5 mg ml^{-1} in PBS) was arrayed onto the porous silicon chips using an in-house developed piezoelectric microdispenser[29,30] forming an array of 600 antibody spots (100 pl/spot), at a 150 μm centre to centre distance. The chips were washed with a 3 time washing step in PBS–Tween (0.05% Tween 20 in PBS) to remove loosely bound capture antibodies. Finally, blocking with 5% non-fat powdered milk was done prior to the insertion of the porous silicon chips to the IAI platform.

Microarray analysis. A confocal microscope setup (BX51W1, Olympus) with oil immersion 20× objective and an ion laser (IMA101010BOS, Melles Griot Laser Group) with an excitation wavelength of 488 nm was used for fluorescence detection. Microarray image analysis was performed using Fluoview 300 software (Fluoview, Olympus). The Fluoview 300 circle method was used to quantify the total intensity of each spot that was detected on the microarray. Background intensity was similarly measured and then subtracted from the total intensity of the spot. Nine spots and their backgrounds were measured for each image analysis, generating the mean spot intensities presented in the figures.

Results and discussion

Optimisation of flow-based microarray assay

The continuous flow-based incubation of the microarray on the IAI platform offers different conditions for the plasma biomarkers to reach the immobilized antibodies on the porous silicon surface as compared to the previously reported microtitre plate-based porous silicon microarray assay.[31] In order to optimize the sample incubation process in the IAI platform, PSA immunoaffinity-capturing was performed at incubation times ranging from 10–30 min. Obtained data showed that 15 min of PSA-spiked plasma perfusion was sufficient for PSA to bind to the immobilized anti-PSA H117 antibody in the continuous flow system, in the range of clinically relevant levels (4–300 ng ml^{-1}), Fig. 2.

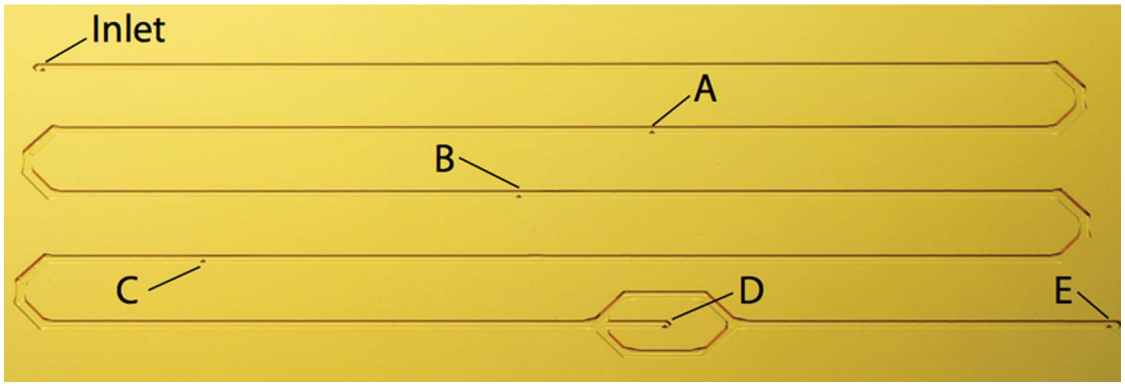

Fig. 1 The acoustic plasmapheresis microchip with multiple outlet configuration (A–D) along the meander shaped separation microchannel for RBC removal and (E) extraction of pure plasma.

To optimize the washing steps in the PSA assay, after the plasma incubation, 5 min washings at flow rates of 50, 100, 200, 500 and 1000 µl min^{-1} were investigated. Based on the spot intensity profiles obtained by microarray image analysis, the results show that a flow rate of 1000 µl min^{-1} (0.05% Tween 20 in PBS) was sufficient to reduce background noise (Fig. 3).

Whole blood analysis

One significant step towards more advanced POC diagnostics includes miniaturization of the conventional immunoassays. In this respect, we evaluated the applicability of the IAI platform to assay PSA, using female plasma samples spiked with PSA.

The plasmapheresis microchip was modified relative our earlier generation to improve the plasma separation/generation and enable integration with the microarray flow cell. The plasmapheresis chip was slightly elongated with a separation channel length of 238 mm (compared to 224 mm in earlier

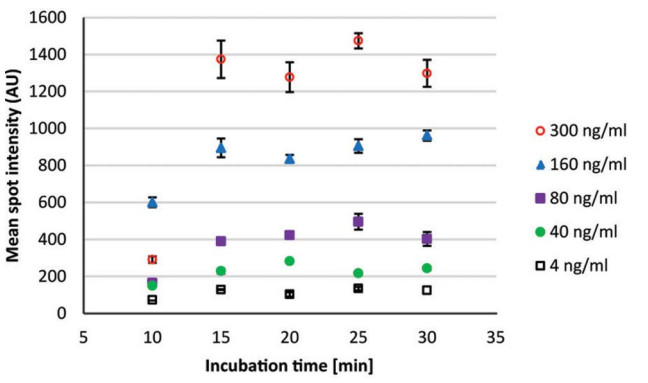

Fig. 2 Fluorescence detection results for PSA-spiked female plasma samples. PSA-spiked plasma perfused a flow cell holding the porous silicon antibody microarray for 10, 15, 20, 25 and 30 min (x-axis) to optimize the continuous flow PSA assay. Mean spot intensities (y-axis) and standard deviation (error bars) were calculated from spots (n = 9) obtained from microarray image analysis. Note that incubation times of more than 15 min did not result in a significantly higher mean spot intensity, thus this time was selected for the subsequent IAI protocol.

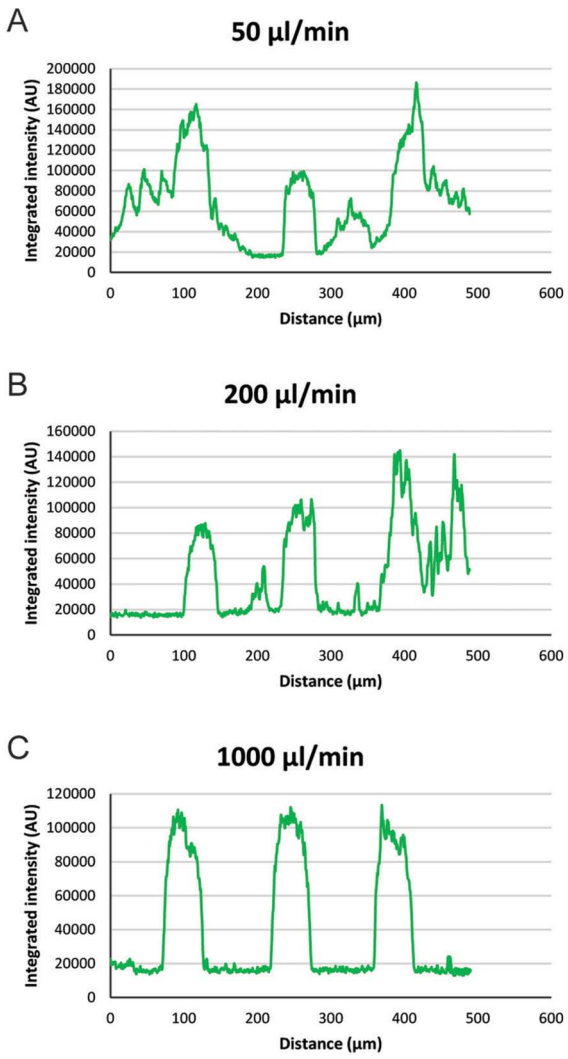

Fig. 3 Spot intensity profiles obtained *via* microarray image analysis. Washing buffer (0.05% Tween 20 in PBS) was aspirated through the microarray flow cell at various flow rates for 5 min. Representative spot profiles for 50, 200 and 1000 µl min^{-1} are shown.

Fig. 4 Sequence showing the starting phase of plasma production A) where ultrasound is inactive, B) where the acoustophoresis is beginning to focus the RBC in the channel centre and C) continuous phase of plasma production where the final fractions of RBC are removed *via* the central outlet.

design), while having the same number of outlets. The microchip was placed in a manifold to couple the plasma microchannel outlet into the flow cell holding the porous silicon microarray chip. PSA-spiked undiluted whole blood was drawn through the acoustic plasmapheresis chip by software-controlled syringe pumps (neMESYS, Cetoni, GmbH, Germany). The acoustophoresis chip was actuated according to the previously described protocol,[24] and hence a half wavelength ultrasonic standing wave was used to accomplish on-chip separation of anti-coagulated plasma from red and white blood cells.[32–34] As seen in Fig. 4, the primary acoustic radiation force focuses the blood cells into the pressure node of the standing wave field, moving them to the centre of the microfluidic channel, while a cell free plasma emerges along the channel sidewalls. Lower flow rates were applied in all waste outlets (outlet A–D) as compared to the earlier design, see Table 1. This contributed to a longer retention time for acoustic focusing and hence improved the plasma separation efficiency. The lower total flow rate of the acoustic plasmapheresis microchip also resulted in lower consumption of whole blood sample.

To remove the focused blood cells from the plasma, these were aspirated through the waste outlet A–D located in the bottom centre of the microchannel (Fig. 1). The sequential removal of focused blood cells *via* multiple outlets along the bottom center of the microfluidic channel gradually reduced the hematocrit level. The trifurcation at the end of the microchannel provided the final cell separation, yielding high quality plasma with a low cellular content through the side outlets. The plasma was generated at a rate of 10 μl min^{-1} from undiluted whole blood (38–40% hematocrit) with a flow rate of 50 μl min^{-1}, as compared to 80 μl min^{-1} in the earlier version. A higher plasma yield of 33% of the total plasma volume was achieved, compared to the 21% for the previous generation. Flow rate settings, plasma yield and plasma cell count are given in Table 1. The plasma generated in the new set-up showed a slightly higher cell content than previous version, which can be attributed to the fact that a larger fraction of the total plasma volume is extracted for the diagnostic step. It should, however, be mentioned that the cell background was still well within the criterion of $< 6 \times 10^9$ cells L^{-1}, as recommended by the Council of Europe.[35]

Increasing the extracted plasma fraction inherently increases the risk of having a carry-over of cells. It should also be noted that the entire plasma volume in a blood sample is not accessible using the acoustophoresis-based approach described herein since the blood cells are not exposed to forces of the same magnitude as in a centrifugation step, and hence are not as densely packed. By exposing the blood sample to the acoustic force field for a longer time, it may be possible to concentrate the blood cells more and thus accomplish a higher plasma fraction yield, but at the cost of either a longer separation channel, a higher acoustic input power or a lower flow rate.

Fig. 5 A–E shows the acoustic plasmapheresis microchip mounted in the manifold that connects the plasma microchannel outlet to the flow cell holding the immunoaffinity-capture microarray (Fig. 5 B–C). Because of the high surface area contributed by the porous silicon 3D morphology, spots with high antibody density and quality were obtained.[36,37] *Via* outlet E, clean plasma continuously perfused the microarray flow cell. After 15 min of continuous flow plasma incubation, the washing buffer (0.05% Tween 20 in PBS) was subsequently aspirated through the flow cell. After incubation, the PSA microarray was subjected to off-line 10 μl FITC-labeled secondary antibody incubation and fluorescence detection. The on-line processing and the short (15 min) PSA immunoaffinity-capture time could reduce the risk of plasma

Table 1 Flow rates for inlet and outlets A–E, plasma yield and the amount of cells L^{-1} of the generated plasma for the improved acoustic plasmapheresis microchip as compared to our previously reported microchip design

	Inlet (μl min^{-1})	Waste outlet A (μl min^{-1})	Waste outlet B (μl min^{-1})	Waste outlet C (μl min^{-1})	Waste outlet D (μl min^{-1})	Plasma outlet E (μl min^{-1})	Fraction of plasma from whole blood	Erythrocytes/L in produced plasma
Previous design	80	20	20	15	15	10	12.5%	3.7×10^9
Improved design	50	10	10	10	10	10	20%	4.2×10^9

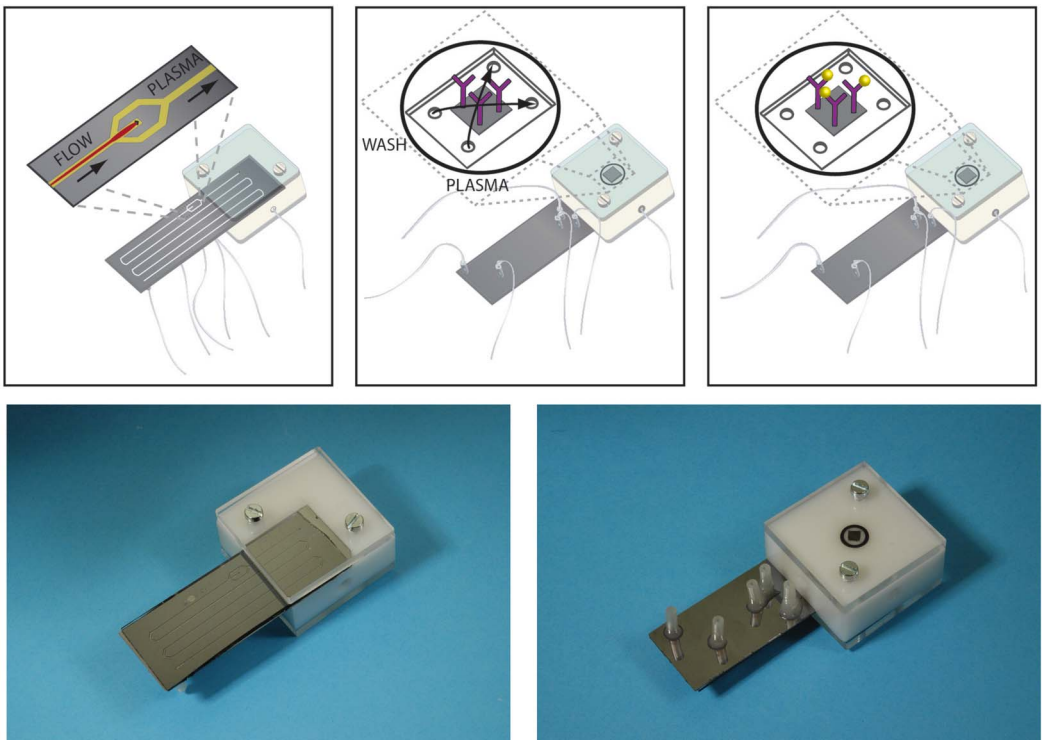

Fig. 5 The Integrated Acoustic Immunoaffinity-capture (IAI) platform. The plasma microchannel outlet is connected to the flow cell containing the porous silicon immunoaffinity-capture region which is perfused by the acoustophoretically generated plasma for 15 min. A) The acoustophoresis-based plasma separation region. B) The porous silicon immunoaffinity-capture microarray region at the back side of the IAI manifold containing the microarrayed anti-PSA H117 antibody (in purple). C) Immunoaffinity-capture of PSA (in yellow) by the anti-PSA H117 antibody. D) Photo of the IAI manifold. E) Photo of the IAI manifold (back side).

protein degradation induced by the standard blood pre-processing and extended time before analysis.[38] Hence, this approach opens the route to more accurate assaying of other more delicate biomarkers.

The IAI protocol for whole blood samples spiked with PSA generated high quality, homogeneous spots (Table 2). An example of a spot intensity profile obtained from the porous silicon PSA microarray can be seen in Fig. 6A. Fig. 6B shows the effect of non-optimal manual washing steps which was successfully eliminated *via* automated and reproducible aspiration of washing buffer on the IAI platform. The mean spot intensities and coefficient of variation (CV) in Table 2 were calculated from the spots of the inset images in Fig. 7. CVs of ~13% are in agreement with previously published work.[28] The graph in Fig. 7 shows mean spot intensity *versus* PSA concentration as determined by the DELFIA reference assay. This corresponded to a coefficient of determination of $R^2 > 0.99$, indicating a good linearity within the studied concentration range. The error bars show the standard deviations calculated from the spot intensities. Based on duplicate runs of the IAI protocol, PSA was detectable at clinically significant levels of 1.7–100 ng ml^{-1} after 15 min of immunoaffinity-capturing at 50 µl min^{-1} total flow rate of whole blood *via* fluorescence readout. Although the lowest concentration measured in blood samples in this study was 1.7 ng ml^{-1}, we have previously shown that the porous silicon sandwich assay used herein has a limit of detection of 0.14 ng ml^{-1} PSA.[28] Unspiked human female whole blood sample was used as a negative control in our experiments. No unspecific binding from plasma proteins was found (data not shown).

Performed as an integrated microfluidic assay, the IAI platform has minimized the number of conventional assay steps, resulting in reduced total assay time and consumption of sample/reagents. Immunoaffinity-capturing of PSA from whole blood, with optimized flow conditions and incubation times, was performed in 15 min as compared to 60 min on our previous PSA microarray platform. The assay steps performed on the IAI (15 min of immunoaffinity-capturing of PSA from whole blood and 5 min washing) lasted for a total of 20 min which should be compared with at least 75 min for the corresponding assay steps performed on our previous PSA microarray platform.

Table 2 PSA concentrations (DELFIA), mean spot intensities, and the corresponding standard deviations and coefficients of variation

Concentration, ng ml^{-1}	Mean spot intensity, AU	Standard deviation, AU (n = 9)	CV% (n = 9)
100	2983	507	17
75	2116	133	6.3
21	660	42	6.3
4	200	26	13.1
1.7	110	22	20.2

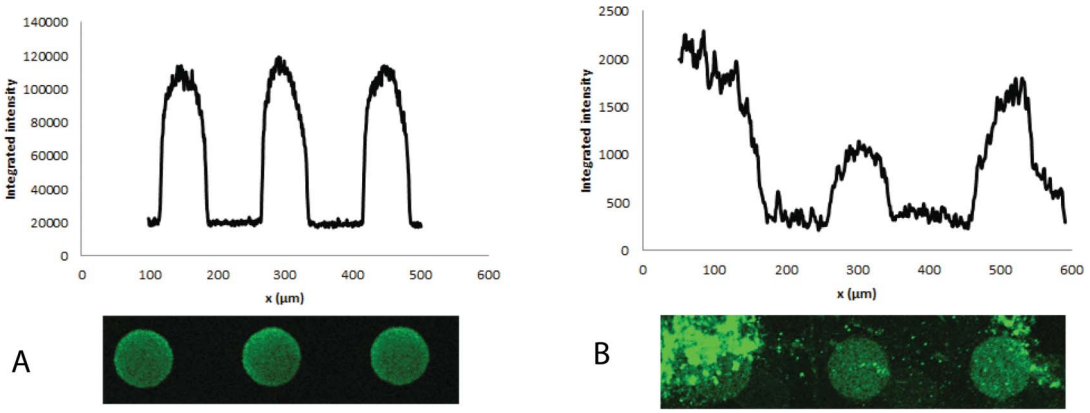

Fig. 6 A) An example of spots and spot intensity profile obtained for PSA detection *via* fluorescence readout on the IAI platform. B) Effect of non-optimal washing steps on the spot profile.

Conclusion

The IAI platform, in its simplest form of integration, has shown proof-of-principle for whole blood sample input and biomarker quantitation output. The platform integrates multiple functions *i.e.* 1) on-chip plasma separation, 2) immunoaffinity-capture and 3) steps of loading samples/reagents/washing buffers. In this paper, we show for the first time microchip integration of acoustically driven plasmapheresis and microarray-based protein biomarker detection, which provides reduced assay times and enables automated microfluidic sample processing.

In upcoming work we anticipate enhancing the diagnostic value in the current PSA microarray by implementing a multiplex microarray holding complementary biomarkers and realizing further steps of integration and miniaturization.

In order to progress the IAI platform to a true sample-in-answer-out point-of-care system, the current off-line incubation of the detector antibody should be integrated into the microfluidic sequence, and this is on-going work. The confocal fluorescence readout can be translated to a conventional bench top fluorescence microarray scanner.

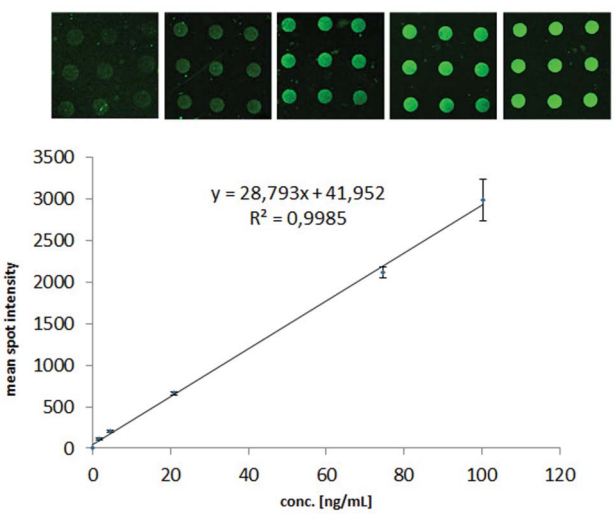

Fig. 7 Fluorescence readout of the titrated series of PSA-spiked female whole blood obtained *via* the IAI protocol. The inset images show microarray images of the corresponding concentration ranges. Mean spot intensities (y-axis) and standard deviations (error bars) were calculated from the spots (n = 9) in the images captured *via* a 20× lens. The PSA concentrations on the x-axis were obtained by the DELFIA reference assay.

Acknowledgements

Financial support is acknowledged from the Swedish Research Council [VR 2009-5361 and VR/Vinnova/SSF MTBH 2006-7600 and K 2009-20095 (Medicine)], the Royal Physiographic Society, the Crafoord Foundation, the Carl Trygger Foundation, the SSF Strategic Research Centre (Create Health), funding (grant no. 11-0624) to H. Lilja from the Swedish Cancer Society, FiDiPro grant support to H. Lilja from TEKES, funds from David H. Koch, provided through the Prostate Cancer Foundation, and the Sidney Kimmel Center for Prostate and Urologic Cancers. National Cancer Institute [grant nos. R33 CA 127768-02, P50-CA92629, R01 CA160816] and the National Institute for Health Research (NIHR) Oxford Biomedical Research Centre based at Oxford University Hospitals NHS Trust and University of Oxford, and Fundación Federico SA.

References

1 N. L. Anderson and N. G. Anderson, *Mol. Cell. Proteomics*, 2002, **1**, 845–867.
2 M. Toner and D. Irimia, *Annu. Rev. Biomed. Eng.*, 2005, **7**, 77–103.
3 J. T. Lathrop, N. L. Anderson, N. G. Anderson and D. J. Hammond, *Curr. Opin. Mol. Ther.*, 2003, **5**, 250–257.
4 R. R. Drake, L. Cazares and O. J. Semmes, *Proteomics: Clin. Appl.*, 2007, **1**, 758–768.
5 H. Jiang, X. A. Weng and D. Q. Li, *Microfluid. Nanofluid.*, 2011, **10**, 941–964.

6 E. Stern, A. Vacic, N. K. Rajan, J. M. Criscione, J. Park, B. R. Ilic, D. J. Mooney, M. A. Reed and T. M. Fahmy, *Nat. Nanotechnol.*, 2010, **5**, 138–142.
7 M. Kersaudy-Kerhoas, D. M. Kavanagh, R. S. Dhariwal, C. J. Campbell and M. P. Y. Desmulliez, *Lab Chip*, 2010, **10**, 1587–1595.
8 W. W. Chen, T. S. Li, S. He, D. B. Liu, Z. Wang, W. Zhang and X. Y. Jiang, *Sci. China: Chem.*, 2011, **54**, 1227–1232.
9 J. Wang and M. P. Chatrathi, *Anal. Chem.*, 2003, **75**, 525–529.
10 C. D. Garcia and C. S. Henry, *Analyst*, 2004, **129**, 579–584.
11 D. Huckle, *Expert Rev. Med. Devices*, 2006, **3**, 421–426.
12 D. Huckle, *Expert Rev. Mol. Diagn.*, 2008, **8**, 679–688.
13 K. Hosokawa, M. Omata and M. Maeda, *Anal. Chem.*, 2007, **79**, 6000–6004.
14 A. Hatch, A. E. Kamholz, K. R. Hawkins, M. S. Munson, E. A. Schilling, B. H. Weigl and P. Yager, *Nat. Biotechnol.*, 2001, **19**, 461–465.
15 T. K. Lim, H. Ohta and T. Matsunaga, *Anal. Chem.*, 2003, **75**, 3316–3321.
16 O. Hofmann, G. Voirin, P. Niedermann and A. Manz, *Anal. Chem.*, 2002, **74**, 5243–5250.
17 U. Y. Schaff and G. J. Sommer, *Clin. Chem.*, 2011, **57**, 753–761.
18 L. Riegger, M. Grumann, T. Nann, J. Riegler, O. Ehlert, W. Bessler, K. Mittenbuehler, G. Urban, L. Pastewka, T. Brenner, R. Zengerle and J. Ducree, *Sens. Actuators, A*, 2006, **126**, 455–462.
19 R. Fan, O. Vermesh, A. Srivastava, B. K. H. Yen, L. D. Qin, H. Ahmad, G. A. Kwong, C. C. Liu, J. Gould, L. Hood and J. R. Heath, *Nat. Biotechnol.*, 2008, **26**, 1373–1378.
20 A. W. Browne, L. Ramasamy, T. P. Cripe and C. H. Ahn, *Lab Chip*, 2011, **11**, 2440–2446.
21 S. Thorslund, O. Klett, F. Nikolajeff, K. Markides and J. Bergquist, *Biomed. Microdevices*, 2006, **8**, 73–79.
22 D. Y. Stevens, C. R. Petri, J. L. Osborn, P. Spicar-Mihalic, K. G. McKenzie and P. Yager, *Lab Chip*, 2008, **8**, 2038–2045.
23 L. D. Qin, O. Vermesh, Q. H. Shi and J. R. Heath, *Lab Chip*, 2009, **9**, 2016–2020.
24 A. Lenshof, A. Ahmad-Tajudin, K. Järås, A. M. Sward-Nilsson, L. Aberg, G. Marko-Varga, J. Malm, H. Lilja and T. Laurell, *Anal. Chem.*, 2009, **81**, 6030–6037.
25 K. Pettersson, T. Piironen, M. Seppala, L. Liukkonen, A. Christensson, M. T. Matikainen, M. Suonpaa, T. Lovgren and H. Lilja, *Clinical Chemistry*, 1995, **41**, 1480–1488.
26 H. Lilja, A. Christensson, U. Dahlen, M. T. Matikainen, O. Nilsson, K. Pettersson and T. Lovgren, *Clinical Chemistry*, 1991, **37**, 1618–1625.
27 K. Mitrunen, K. Pettersson, T. Piironen, T. Bjork, H. Lilja and T. Lovgren, *Clinical Chemistry*, 1995, **41**, 1115–1120.
28 K. Järås, A. Ressine, E. Nilsson, J. Malm, G. Marko-Varga, H. Lilja and T. Laurell, *Anal. Chem.*, 2007, **79**, 5817–5825.
29 T. Laurell, L. Wallman and J. Nilsson, *J. Micromech. Microeng.*, 1999, **9**, 369–376.
30 P. Onnerfjord, J. Nilsson, L. Wallman, T. Laurell and G. Marko-Varga, *Anal. Chem.*, 1998, **70**, 4755–4760.
31 K. Järås, B. Adler, A. Tojo, J. Malm, G. Marko-Varga, H. Lilja and T. Laurell, *Clin. Chim. Acta*, 2012, **414**, 76–84.
32 A. Nilsson, F. Petersson, H. Jonsson and T. Laurell, *Lab Chip*, 2004, **4**, 131–135.
33 J. J. Hawkes, R. W. Barber, D. R. Emerson and W. T. Coakley, *Lab Chip*, 2004, **4**, 446–452.
34 N. R. Harris, M. Hill, S. Beeby, Y. Shen, N. M. White, J. J. Hawkes and W. T. Coakley, *Sens. Actuators, B*, 2003, **95**, 425–434.
35 R. Cardigan, *Guide to the Preparation, Use and Quality Assurance of Blood Components*, Council of Europe Publishing, Strasbourg, 13th edn, 2007.
36 A. Ressine, S. Ekström, G. Marko-Varga and T. Laurell, *Anal. Chem.*, 2003, **75**, 6968–6974.
37 C. Steinhauer, A. Ressine, G. Marko-Varga, T. Laurell, C. A. K. Borrebaeck and C. Wingren, *Anal. Biochem.*, 2005, **341**, 204–213.
38 S. Y. Hsieh, R. K. Chen, Y. H. Pan and H. L. Lee, *Proteomics*, 2006, **6**, 3189–3198.

